Computers in Biology and Medicine 196 (2025) 110545

Contents lists available at ScienceDirect

Computers in Biology and Medicine

journal homepage: www.elsevier.com/locate/compbiomed

Morphological inhibitors of aggregation-prone amyloid-β conformers: A computational exploration

Stefano Bosio [a,b,1], Federico Falchi [a,b,1], Chiara Rauzi [a], Luca Bellucci [c,*]

[a] Department of Pharmacy and Biotechnology, Alma Mater Studiorum - University of Bologna, Via Belmeloro 6, 40126 Bologna, Italy
[b] Computational and Chemical Biology, Italian Institute of Technology, Via Morego 30, 16163 Genova, Italy
[c] Istituto-Nanoscienze del Consiglio Nazionale delle Ricerche (CNR-NANO), NEST-SNS, Piazza San Silvestro 12, 56127 Pisa, Italy

ARTICLE INFO

Keywords:
Amyloid-β
Alzheimer's disease
Intrinsically disordered proteins
Amyloid-β aggregation
Aggregation inhibitors
Molecular dynamics

ABSTRACT

Alzheimer's disease is a neurodegenerative disorder characterized by progressive cognitive decline and memory loss. It is associated with the self-assembly of the amyloid-β peptide, a soluble intrinsically disordered protein naturally present in the brain parenchyma in various alloforms. This study presents a computational approach to identify possible modulators of the monomeric aggregation-prone conformations of amyloid-β, a critical intermediate in the fibrillation process. A structure-based virtual screening campaign was designed using a structural ensemble to identify potential binders. The workflow included binding site identification, small molecule–peptide docking, protein–protein docking, and molecular dynamics simulations to evaluate interaction stability and aggregation propensity. From this pipeline, a set of novel molecules was identified as capable of interacting with aggregation-prone forms of amyloid-β, potentially reducing their tendency to form toxic aggregates.

1. Introduction

Alzheimer's disease (AD) is a widespread neurodegenerative disorder characterized by progressive cognitive decline and memory loss. As the most common form of dementia, AD affects millions of people worldwide, with its prevalence expected to rise in the coming decades due to the increase in life expectancy and the aging global population [1]. The pathogenesis of AD is complex and multifactorial, involving several biological mechanisms among which the self-assembly of the amyloid-*beta* (Aβ) peptides plays a central role in disease progression. Aβ peptides are intrinsically disordered proteins (IDPs) naturally present in the brain parenchyma in various alloforms, among which Aβ 1–42 (Aβ42) is considered the most cytotoxic [2]. In physiological environments, Aβ monomers, as IDP, lack a fixed three-dimensional structure and instead exist as dynamic ensembles of inter-converting structural states [3].

The amyloid cascade hypothesis proposes that the neurodegenerative process in AD is initiated by the accumulation of Aβ oligomeric and fibrillar forms. These aggregated species are thought to disrupt neuronal function and synaptic plasticity, which are critical for learning and memory [4]. This hypothesis highlights the key role of Aβ aggregation in disease progression, associating toxic assemblies with the cognitive impairments observed in AD patients [5,6]. The self-assembly of Aβ generally involves several interconnected processes. These processes begin with a primary nucleation step, progress through the formation of disordered oligomers, and convert into growth-competent nuclei that eventually elongate into fibrillar assemblies. From a molecular point of view, monomeric units can coexist, but under certain conditions, for instance an increased concentration, they begin to aggregate into small oligomers [5,7]. These oligomers can interact with each other or with additional monomers, eventually leading to the formation of insoluble amyloid fibrils [5,7]. Despite being soluble, Aβ oligomers have emerged as important factors in neurotoxicity [8]. These structures are implicated in triggering multiple toxic mechanisms, including synaptic dysfunction, compromised membrane integrity, oxidative damage, impaired mitochondrial function, and enhancement of inflammatory responses [9–11]. Although the precise mechanism of Aβ self-assembly remains unclear, fibrillation is known to be influenced by various environmental factors, including peptide concentration, pH, presence of biomolecules, metal ions and nanoparticles [12–21]. Therefore, the inherent conformational dynamics makes the fibrillation process of IDPs particularly susceptible to environmental conditions. Based on these findings, several strategies have been developed to influence the equilibrium of Aβ monomers in solution. Among these, immunotherapies targeting Aβ, including monoclonal antibodies such as Donanemab

* Corresponding author.
E-mail address: luca.bellucci@nano.cnr.it (L. Bellucci).
[1] These authors contributed equally to this work.

https://doi.org/10.1016/j.compbiomed.2025.110545
Received 10 February 2025; Received in revised form 2 June 2025; Accepted 3 June 2025
Available online 4 July 2025

and Aducanumab, have demonstrated the potential of these therapeutic approaches [22]. Both antibodies target toxic Aβ conformations, with Donanemab acting on both soluble and insoluble plaques, while Aducanumab specifically binds to aggregated forms [23–26]. While immunotherapies have demonstrated potential in reducing β-amyloid accumulation, their application is limited due to challenges associated with intravenous administration. For many years, attempts to treat AD with small molecules primarily focused on disease modification or symptoms [27]. However, recent advances have introduced novel strategies that show promising results. These include the use of small molecules designed to disrupt early aggregation-prone conformations of Aβ[28,29] or to enhance the structural variability of Aβ, thus stabilizing its non-toxic conformations through transient interactions [30–35]. Therefore, targeting these transient states that display features associated with fibrillation propensity through small molecules capable of preventing the transition from non-toxic peptide conformations to more aggressive fibrillar forms may represent an effective strategy to block the early stages of amyloid formation and slow the progression of Alzheimer's disease. Hereafter, we use the term "fibrillar-prone" or "aggregation-prone" conformations to describe these transient Aβ states, which are structurally characterized by reduced solvent exposure and non-globular shape. These are structural features known to statistically bias the peptide toward fibril aggregation [36,37]. Such approaches offer the advantage of potentially bypassing the pharmaceutical challenges associated with antibody-based therapies. Interestingly, an intermediate strategy using peptides to destabilize aggregated forms of Aβ is also under investigation. One such peptide-based therapeutic, namely PRI-002, has progressed to phase II clinical trials, further highlighting the heterogeneity of approaches being explored to address Aβ aggregation [38,39].

In this study, we explored the dynamic nature of Aβ in solution, using a structural ensemble characterized in a previous work [13] to account for the intrinsic flexibility and diverse conformational states of Aβ, providing a realistic representation of the target. Representative conformations of the Aβ peptide were selected from these long simulations, focusing on states prone to form toxic oligomers based on structural parameters. Remarkably, these representative conformations were subjected to rigid homodimer docking, and the associated scoring functions were used to assess their aggregation tendency, providing a descriptor that enables the classification of conformers as aggregation-prone or non-aggregation-prone. While previous studies have primarily investigated the aggregated forms of Aβ and demonstrated promising results in disrupting these structures [28,29,40], the critical step in AD pathogenesis is the transition of Aβ from a stable, non-toxic, ensemble of conformations into fibrillation-prone intermediates. Moreover, several computational studies have helped clarify the inhibitor mechanisms of a range of small molecules targeting Aβ [41–46]. These studies highlighted the utility of MD simulations and related in silico methodologies for the detailed characterization of Aβ binding modes and for the rational design of aggregation inhibitors. For this reason, our aim was to target early-stage fibrillation-prone conformations and elongated forms of Aβ were chosen as the primary targets of our drug discovery campaign. Specifically, we aimed to identify small molecules capable of selectively binding to these transient states, thereby inhibiting their progression into toxic oligomers. Finally, eight molecules were identified and characterized as potential binders and inhibitors of the fibrillar-prone forms of amyloid-β.

2. Method and computational details

2.1. Representative structure selection and characterization

The configurations analyzed in this study were derived from simulations conducted by Bellucci et al. [13]. That work extensively characterized the conformational ensemble of Aβ42 in an aqueous solution using temperature replica exchange molecular dynamics (T-REMD) simulations [47] and OPLS force field [48,49]. To consider the potential interconversion among various conformational states, which may occur via extended intermediates, the T-REMD simulation was executed using a cubic box with dimensions of 7.2 nm per side. This box was sufficiently sized to enable the sampling of elongated conformers [50] (Refer to the "Methods" section of [13] for further details). The simulation of Aβ identified 484 clusters using a Cα-RMSD threshold of 0.28 nm, revealing the diverse conformational ensemble of Aβ in water. Aβ was mostly globular in bulk water, but approximately 10% of the conformations were elongated, with a radius of gyration (R_g) exceeding 1.1 nm; these elongated forms have been linked to fibrillar-prone states, as demonstrated in the original study [13].

Representative structures were extracted from simulation representatives, focusing on conformations intermediate between globular and fibrillar states. The classification of these intermediates was based on two key structural metrics: R_g and the solvent-accessible surface area (SASA). These parameters provided robust criteria for identifying relevant configurations for further analysis. In fact, a R_g greater than 1.1 nm was chosen to identify elongated structures, while a SASA value above 36 nm^2 was used to select structures with large exposed surfaces, which are known to resemble conformations prone to fibrillation, consistently with what is reported in [13]. To identify a transient binding site suitable for docking experiments, the SiteMap tool [51,52] was used with permissive parameters, enabling the identification of shallow pockets. The selected structures were used as input for HADDOCK [53] to perform docking of two identical copies for each of the selected structures. The web server for integrative modeling of biomolecular complexes [54], with the default setup, was used to perform all docking calculations. The scoring obtained was associated with the binding free energy of the complex and can be employed to assess the aggregation propensity of a given structure, thus characterizing the selected structures with respect to their fibrillation propensity (See Fig. 1 left side).

2.2. Virtual screening database preparation

A 3D molecular database was constructed using the Schrödinger Suite (Schrödinger Release 2023-2), starting from 2D structures obtained from two vendors: LifeChemical (http://www.lifechemicals.com/) and Asinex (http://www.asinex.com/). The 2D structures were converted into 3D representations, and stereoisomers were generated using LigPrep (Schrödinger Release 2023-2: LigPrep, Schrödinger, LLC, New York, NY, 2023). All possible ionization states at pH 7 ± 1, along with tautomers, were generated using Epik [55]. The resulting database consisted of approximately 1.2 million compounds.

To enhance the pharmaceutical profile of the database, compounds containing PAINS (Pan-Assay Interference Compounds), metal ions, or more than two stereocenters were excluded. Furthermore, since the target is localized in the central nervous system, the filtered compounds were further screened for their ability to cross the blood–brain barrier (BBB) using descriptors available in QikProp (Schrödinger Release 2023-2: QikProp, Schrödinger, LLC, New York, NY, 2024). The final set after the filtering stage consisted of 410,000 molecules.

2.3. Protein preparation and virtual screening

Virtual screenings were conducted using Maestro Schrödinger version 2023-4. The selected structures were prepared using the Protein Preparation Wizard (Schrödinger, LLC, New York, NY, 2023), which includes Epik and Prime modules. For each representative structure, grids were generated using inner and outer boxes of 10 Å and 30 Å, respectively. These grids were centered on the geometric center of the identified binding sites, ensuring comprehensive coverage and sufficient flexibility for ligand sampling during docking. A hierarchical docking workflow was employed to efficiently screen and refine potential binders [56,57].

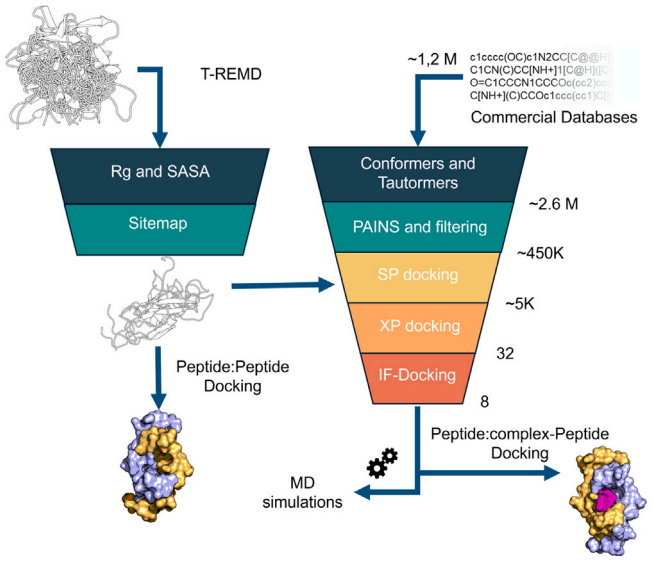

Fig. 1. Computational workflow for identifying potential morphological inhibitors of Aβ aggregation. The workflow integrates peptide conformation selection and characterization using R_g, SASA, Sitemap analysis to find and characterize the binding pocket, and evaluation of homodimer formation via peptide-peptide docking (left side). On the right side, virtual screening over selected structures includes filtering by conformers, tautomers, Pan-Assay Interfering Substances (PAINS), and metals, followed by SP docking, XP docking, and induced-fit (IF) docking. The final stage involves characterizing peptide–inhibitor complexes achieved through molecular dynamics simulations of the complexes and docking analyses of the peptide and its peptide–inhibitor complexes.

The process began with an initial screening using the Standard Precision (SP) scoring function as implemented in Glide [58–61] to evaluate the entire database. Top-ranking compounds were selected for further analysis.

This subset of compounds was visually examined to confirm their compatibility with the binding site. The remaining compounds were then re-docked using the Extra Precision (XP) scoring function available in Glide [58–61], allowing for a more accurate consideration of solvation effects and protein–ligand interactions. Finally, the top scoring molecules were further analyzed with an Induced-Fit Docking instance (See Fig. 1 right side). The induced-fit docking poses were interpreted as interaction models that suggest likely anchoring points, given the impossibility of defining definitive stable binding modes for an IDP.

2.4. Molecular dynamics simulations

Molecular dynamics (MD) simulations of Aβ with selected ligands were performed with the primary objective of characterizing local structural rearrangements within the complex and analyzing the interaction between the components of the system, rather than exhaustively exploring the conformational landscape of the complexed Aβ. For this reason, relatively short simulation times and a reduced box size were employed.

All simulations were performed using the Desmond molecular dynamics (MD) software engine [62], as provided in the Maestro suite. The systems were prepared using the Maestro system builder interface. Each complex was solvated in an orthorhombic periodic box filled with water molecules, ensuring a minimum distance of 15 Å between the solute and the edges of the box. The OPLS4 force field [48] was used for the protein and ligand, while the TIP3P model [63] was used for water. The use of the OPLS4 force field was motivated by the need to maintain consistency with the force field employed to generate the conformational dataset in the previous MD simulation [13]. Coulomb and Lennard-Jones short interactions were truncated with a cutoff distance of 10 Å. The long-range electrostatic interactions were computed using the smooth particle mesh Ewald (SPME) algorithm as implemented in Desmond. The RESPA integrator [64] was used, using a time step of 2 fs for short-range forces and 4 fs for long-range ones. Water molecules were treated as rigid, and all hydrogen bonds to their bonded atoms were constrained.

All systems were minimized and relaxed using the standard relaxation protocol implemented in Maestro. For each system, four independent runs of 200 ns each were performed to ensure statistical robustness in analyzing the dynamic stability of the complexes. Production runs were performed in the NPT ensemble and the trajectories were saved every 25 ps. The Nosé–Hoover chains [65] was used to control the temperature at the reference value of 300 K while constant pressure was maintained at 1 atm using the Martyna–Tobias–Klein Barostat [66].

2.5. MM-GBSA analysis

Molecular Mechanics Generalized Born Surface Area (MM-GBSA) [67] was used to estimate the binding free energy of complexes. This model combines the OPLS-AA force field [48], an implicit solvent model, and corrections for hydrogen bonding, π–π interactions, self-contact, and hydrophobic effects (see section "MM-GBSA details" in SI for more details). MM-GBSA calculations were interpreted in a comparative manner to evaluate the interaction energies of the complexes, focusing on relative differences between poses within the same conformational ensemble. This approach provides a range of interaction confidence rather than relying on absolute energy values.

3. Results

To identify potential morphological inhibitors of Aβ aggregation, a computational workflow was used that combined peptide conformation selection, site evaluation, and virtual screening (Fig. 1). The process begins with the selection of Aβ conformations based on structural characteristics, along with the binding pockets detection and analysis. Peptide-peptide docking is then performed to evaluate the formation of homodimer peptide-peptide complexes, which are linked to their propensity to initiate amyloidogenesis (Fig. 1 left side). Virtual screening of small molecules follows over the selected structures. The workflow concludes with the identification and characterization of peptide–inhibitor complexes that interfere with aggregation-prone Aβ conformations(Fig. 1 right side).

3.1. Structure selection

The radius of gyration (R_g) and the solvent-accessible area (SASA) were calculated for each structural representative to identify structures with a more elongated shape. A threshold of 1.1 nm was applied to R_g (Fig. 2A) while a second threshold of 36 nm^2 was imposed on SASA (Fig. 2B). As shown in Fig. 2C, conformations exhibiting higher values for these metrics were underrepresented compared to the overall ensemble. This distribution underscores the limited representation of the elongated structures in the starting conformational ensemble of 484 structures [13]. The fibrillar-prone structures appear to occupy a minority of the conformational space, suggesting their thermodynamic instability.

3.2. Peptide:Peptide docking

The conformations meeting the established criteria were further analyzed to identify candidates suitable for docking studies. From a subset of 32 elongated structures, through visual inspection of the pocket topology, five representative conformations were selected (Fig. 2D). This selection ensured structural diversity among the structures considered, crucial for a solid virtual screening campaign. The selected structures were evaluated for their ability to initiate fibril formation by

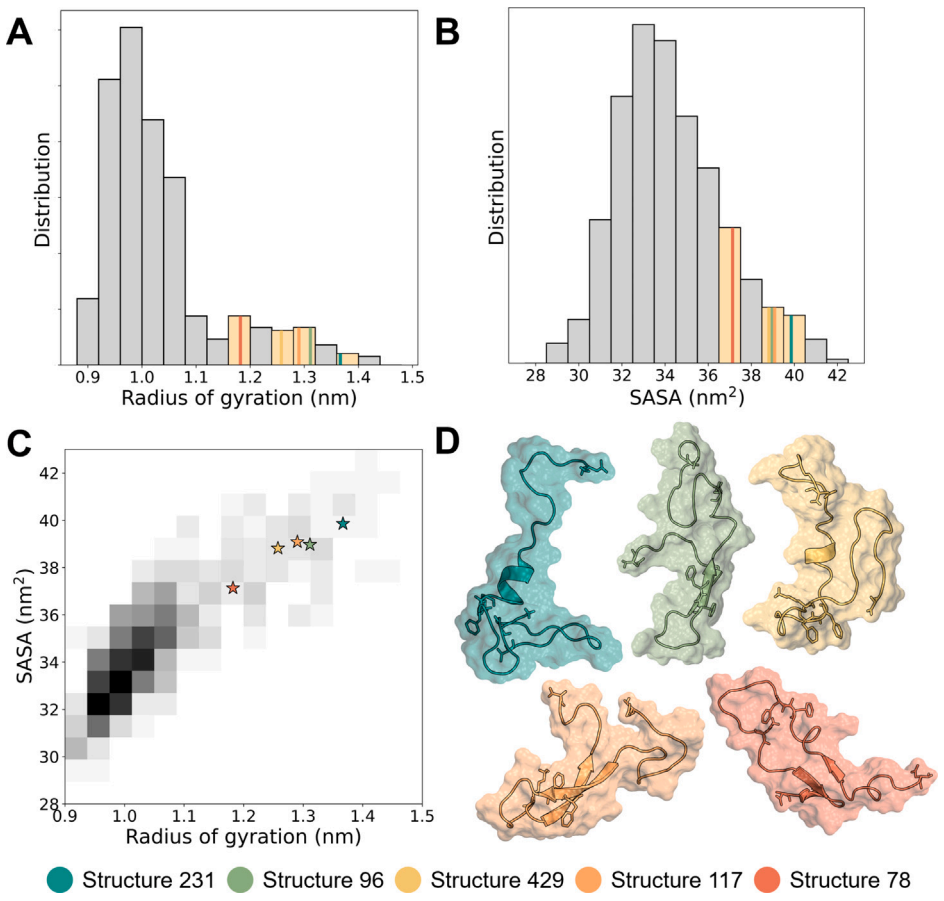

Fig. 2. (A) Distribution of the radius of gyration (R_g) calculated for 484 representative structures, providing insights into their conformational compactness. (B) Distribution of solvent-accessible surface area (SASA) values, reflecting the exposure of structural components to the solvent environment. (C) 2D correlation plot between R_g and SASA, revealing relationships and trends across the dataset. (D) 3D representations of selected structures chosen for detailed investigation. Structures are color-coded as follows: structure 231 (lightblue), structure 96 (green), structure 429 (yellow), structure 117 (orange), and structure 78 (red).

analyzing their self-interactions in order to estimate their homodimerization propensity. These self-interactions were used to define a score that serves as a descriptor of the aggregation propensity of the single peptide, thus representing a necessary, though not sufficient, condition for fibrillogenesis.

This evaluation was performed using the HADDOCK webserver, designed to model protein–protein interactions and estimate their binding affinity via a scoring function [53,54]. As control, we selected a globular conformation having a R_g of 1.02 nm and a SASA of 36.6 nm^2 (see Fig. S1). The selected elongated conformations (yellow bar in Fig. 3) exhibit significantly better HADDOCK scores (H-Scores) than the control structure, suggesting a higher propensity to aggregate compared to the globular reference structure shown in orange on the right. Consistent with our findings, previous works [36,68] proposed that extended or β-hairpin-like Aβ conformations could indeed promote aggregation underscoring that elongated structures are critical intermediates on the aggregation pathway.

Notably, structure 429 showed the greatest tendency to self-assemble, being the most stable homodimer, followed by structures 78, 231, 96, and 117.

3.3. Virtual screening

Virtual screening was conducted to identify small molecules targeting early-stage fibrillation-prone Aβ conformations. Five distinct suitable pockets were identified, one for each structure (See Tab. S2). The selection process considered pocket shape, SiteScore, and Dscore, taking into account the different purpose of these metrics, originally designed for well-structured pockets [51,52]. Detailed scores and metrics for the identified pockets are provided in the Supporting Information (Tab. S2).

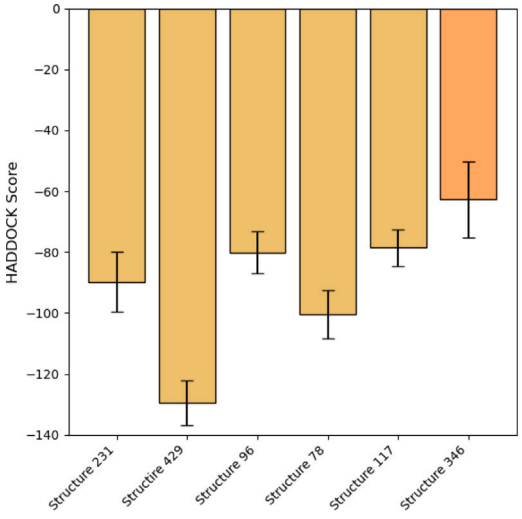

Fig. 3. Histogram of scores obtained from the protein–protein HADDOCK calculations. Initial elongated structures are represented in yellow, whereas a single globular conformations, serving as example that achieves the highest score and highlights its non-fibrillar nature, is in orange. Black error bars indicate variability in the scoring calculations.

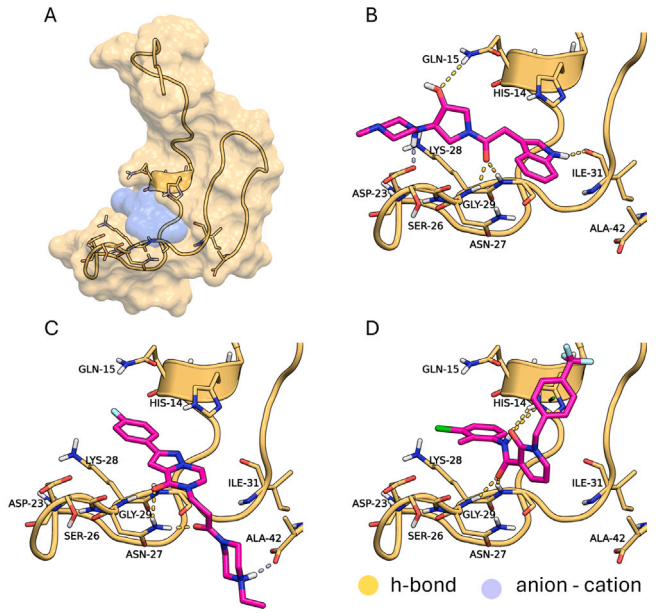

Fig. 4. (A) 3D representation of structure 429, highlighting the potential binding site identified by SiteMap (shown in blue). (B) Key interactions of the small molecule SM1 with the binding site. (C) Key interactions of the small molecule SM2 with the binding site. (D) Key interactions of the small molecule SM3 with the binding site. Protein–ligand interactions are depicted as dashed lines, color-coded according to the interaction type: hydrogen bonds in yellow, anion–cation interactions in light blue. Ligand-interacting residues are labeled for reference.

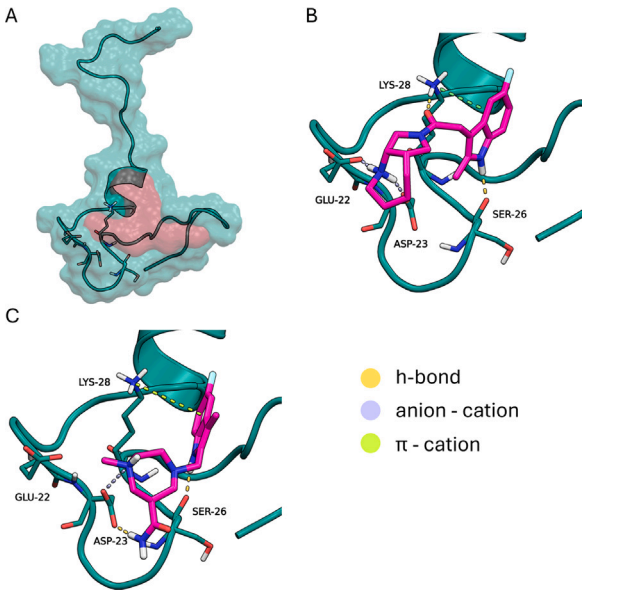

Fig. 5. (A) 3D representation of structure 231, highlighting the potential binding site identified by SiteMap (shown in red). (B) Key interactions of the small molecule SM4 with the binding site. (C) Key interactions of the small molecule SM5 with the binding site. Protein–ligand interactions are depicted as dashed lines, color-coded according to the interaction type: hydrogen bonds in yellow, anion–cation interactions in light blue, π–cation interactions in lime. Ligand-interacting residues are labeled for reference.

The ensemble docking across all structures, performed using virtual screening techniques with criteria as reported in the Methods, identified eight molecules, which are presented in the Supporting Information (Tab. S1,Fig. S2) as SM1 to SM8.

For each of the selected structures, we evaluated both the Glide Score and the residue interactions. Specifically, analysis of the site present on the surface of structure 429 (Fig. 4A) led to the selection of three molecules. In particular, SM1 interacts through a dense network of hydrogen bonds, primarily with the backbone of the structure, as shown in Fig. 4B. Specifically, it forms hydrogen bonds with Ile-31, Gly-29, Gln-15, and Ser-26. In addition, a salt bridge is established with Asp-23. Similarly, SM2 interacts with Gly-29 via two hydrogen bonds that stabilize the core of the molecule (Fig. 4C). This interaction pattern is also preserved in SM3 (Fig. 4D).

The second site was identified on structure 231 Fig. 5A. In this case two molecules, (SM4 and SM5) were selected for further analysis. Notably, SM4 engages in both an ionic interaction and a hydrogen bond with Asp-23. Furthermore, it forms a π–cation interaction with Lys-28 and a hydrogen bond with Ser-26 (Fig. 5B). The second molecule selected for this site, SM5, exhibits similar interaction patterns. It retains the π–cation interaction with Lys-28 and the hydrogen bond with Ser-26. In this case, the ionic interaction can involve both Asp-23 and Glu-22 (Fig. 5C).

From the site identified on the structure 96 (Fig. 6A), we selected three additional ligands. Notably, SM6 interacts through two $\pi - \pi$ interactions with Phe-20 and Tyr-10, leveraging both aromatic rings present in its structure (Fig. 6B). The other ends of the molecule are anchored to the protein via two distinct salt bridges with Asp-7 and Asp-1. Additionally, a hydrogen bond is established between the amidic nitrogen of the ligand and Asp-1.

The interaction pattern is largely preserved across the other selected ligands, SM7 and SM8 (Fig. 6C and D, respectively). Furthermore, SM8 forms two hydrogen bonds with His-14 and Glu-11 (dashed yellow lines in Fig. 6D).

The sites pertaining to structure 117 and structure 78 were excluded due to the lack of compound stability observed during the Induced-Fit

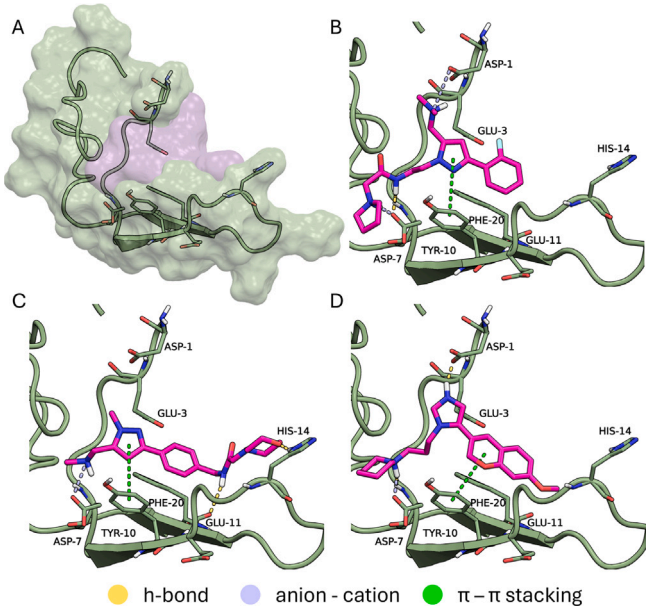

Fig. 6. (A) 3D representation of structure 96, highlighting the potential binding site identified by SiteMap (shown in purple). (B) Key interactions of the small molecule SM6 with the binding site. (C) Key interactions of the small molecule SM7 with the binding site. (D) Key interactions of the small molecule SM8 with the binding site. Protein–ligand interactions are depicted as dashed lines, color-coded according to the interaction type: hydrogen bonds in yellow, anion–cation interactions in light blue, and π–π stacking interactions in green. Ligand-interacting residues are labeled for reference.

Docking phase (see SI "Analysis of Sites 117 and 78" and Fig S3–S4 for more details).

3.4. Peptide:Peptide-SM Docking

The selected compounds, bound to the specific conformation they were docked with, were analyzed using HADDOCK to assess the stability of the ternary complex (i.e. homodimer in presence of the small

Table 1
HADDOCK scores (H-Scores) and relative errors of the complexes. The values for the homodimer complex, consistently exceeding those of the complex between the peptide conformation and the identical peptide conformations bound to the ligand. Scores for homodimer complexes (without ligand) are in bold.

Complex		H-Scores (a.u.)
429	429	**−129.6 ± 7.3**
429	429:SM1	−101.9 ± 3.3
429	429:SM2	−92.0 ± 3.8
429	429:SM3	−80.8 ± 8.2
231	231	**−89.8 ± 9.8**
231	231:SM4	−76.5 ± 6.4
231	231:SM5	−66.3 ± 7.3
96	96	**−80.1 ± 6.8**
96	96:SM6	−73.9 ± 5.0
96	96:SM7	−66.6 ± 7.1
96	96:SM8	−63.2 ± 4.7

molecule). All of the selected compounds demonstrated theoretical ability to reduce binding affinity, as predicted by protein–protein docking analysis. Among these, the complexes formed with structure 429 exhibited the highest degree of binding affinity reduction. In particular, SM3 and SM2 showed a significant effect, while SM1 achieved a lower score (Table 1). For structure 231, SM5 exhibited a stronger effect, whereas the performance of SM4 appeared to fall within the range of statistical error. Finally, for structure 96, SM7 and SM8 displayed better binding affinity scores, while SM6 showed a comparatively weaker effect.

In conclusion, all the selected compounds exhibited the ability to reduce the aggregation propensity of the fibrillar-prone structure (see Fig. S5). This reduction in aggregation potential highlights the capacity of the compound to modulate the dynamic conformational equilibrium of intrinsically disordered proteins, thereby interfering with the early stages of fibril formation.

Analyzing the 3D rearrangements of the dimers formed by both the ligand-bound and unbound structures (Fig. S6) we observed a particular behavior in the complexes of the structure 231 and partially in the complex 96-SM6. Specifically, although the overall dimer arrangement changes between the bound and unbound forms, the interacting surface remains preserved in these two cases. In contrast, all other ligands occupied the previously used protein interface, reducing the available peptide–peptide interface and potentially limiting dimerization.

3.5. Molecular dynamics simulations and binding free energy estimation

The stability and structural evolution of all predicted complexes were assessed through molecular dynamics (MD) simulations, following the protocol described in the Methods section. To enhance the reliability of the MD simulation results, four independent MD simulations were performed for each system. The simulations revealed a diverse behavior in the dynamics of the different complexes, attributed to the extreme flexibility of the Aβ peptide. Given our focus on estimating the binding interactions between the compounds and Aβ across the different conformational states sampled during the evolution of the system, we calculated the MM-GBSA binding affinities for every 10th saved frame of the trajectory (Fig. S7). Overall, MD simulations revealed that the ligands did not maintain a single stable binding mode throughout the simulations. However, they demonstrated adaptability by re-establishing binding interactions, underscoring their potential efficacy in engaging with multiple conformations of the intrinsically disordered Aβ structure. The time series of the evolution of the MM-GBSA, shown in Fig. S7, captures this dynamic behavior between the four replicas of each system, suggesting that critical binding interactions were largely preserved (Tab. S3). In light of the variability observed during the dynamics, data from all four replicas were aggregated to ensure robust statistical analysis, and the distribution of the calculated ΔG values obtained from MM-GBSA is shown in Fig. 7. The mean MM-GBSA values derived from MD simulations for all molecular complexes are presented in Tab. S3. The results revealed distinct trends among the compounds. For SM2, SM3, and SM5, the simulations showed an overall decrease (i.e., improvement) in the binding free energy, indicating enhanced stability of the interactions with Aβ. In contrast, SM4 exhibited relatively stable binding free energy values centered around the mean, suggesting consistent interaction throughout the simulation. However, for SM1, SM6, SM7, and SM8, while the interaction was not entirely lost in some cases, an increase in binding free energy was observed, indicating a weaker or less stable binding affinity under the simulated conditions.

These findings underscore the variability in compound efficacy when interacting with the highly dynamic Aβ conformations. Compounds SM2, SM3, and SM5, in particular, stand out as promising candidates for further investigation due to their favorable binding profiles. In particular, compared to the other compounds, SM2, SM3, and SM5 maintained more stable and persistent interactions with the Aβ monomer throughout the molecular dynamics simulations. Moreover, the MM-GBSA analysis revealed an overall improvement in their binding free energy profiles compared to the initial docking poses, indicating enhanced binding stability.

4. Discussion

The identification of distinct binding pockets across the selected structures underscores the unique challenges associated with targeting disordered systems, such as IDPs, or flexible and dynamic systems, such as small RNA molecules, as highlighted in previous works [34, 69]. Their pronounced flexibility determines significant difficulties for classical structure-based drug discovery programs. In fact, unlike traditional drug discovery targets, these systems require careful consideration of additional factors. Disordered systems, such as the amyloid Aβ monomer in solution, derive their stability from a heterogeneous ensemble of conformations corresponding to multiple and degenerate energy states. This characteristic is crucial because all Aβ conformations in solution are transient and their structural features evolve dynamically over time. Consequently, the presence of a binding mode associated with specific conformations also reflects the dynamic nature of the system and is itself transient. Consequently, both the affinity and the overall stability of a ligand–monomer are dictated by the probability of particular conformational states of the monomer that present specific binding modes. As a result, a ligand must identify suitable conformations from a large ensemble, rather than simply stabilizing a single active or inactive state.

The Aβ monomer has structural features that allow ligand binding, forming transient yet functionally significant complexes. Although these complexes may evolve over time, the recurring contacts between the ligands and Aβ can nevertheless hinder the early stages of fibril formation. Indeed, HADDOCK estimation suggest that the selected molecules, by interacting with specific monomeric conformations, effectively could reduce the propensity of Aβ to aggregate in the initial phase of fibril development. This inhibition may provide critical time for fibrillar-prone monomers to revert to thermodynamically stable conformations within the ensemble, thereby reducing their propensity to aggregate.

This approach highlights the importance of targeting early aggregation events, where monomeric structures play a key role. By stabilizing these intermediates and sterically occupying residues critical for aggregation-prone interactions, the selected compounds can effectively modulate the conformational equilibrium of Aβ. Such modulation reduces the likelihood of oligomer and fibril formation, thus mitigating downstream cellular toxicity. Therefore, we hypothesize that ligand–Aβ interactions deactivate aggregation-prone intermediates by shielding critical interfaces. This obstruction may limit Aβ monomers from forming stable higher-order assemblies. The transient nature of interactions highlights the intrinsic challenge of targeting IDPs. Their flexibility

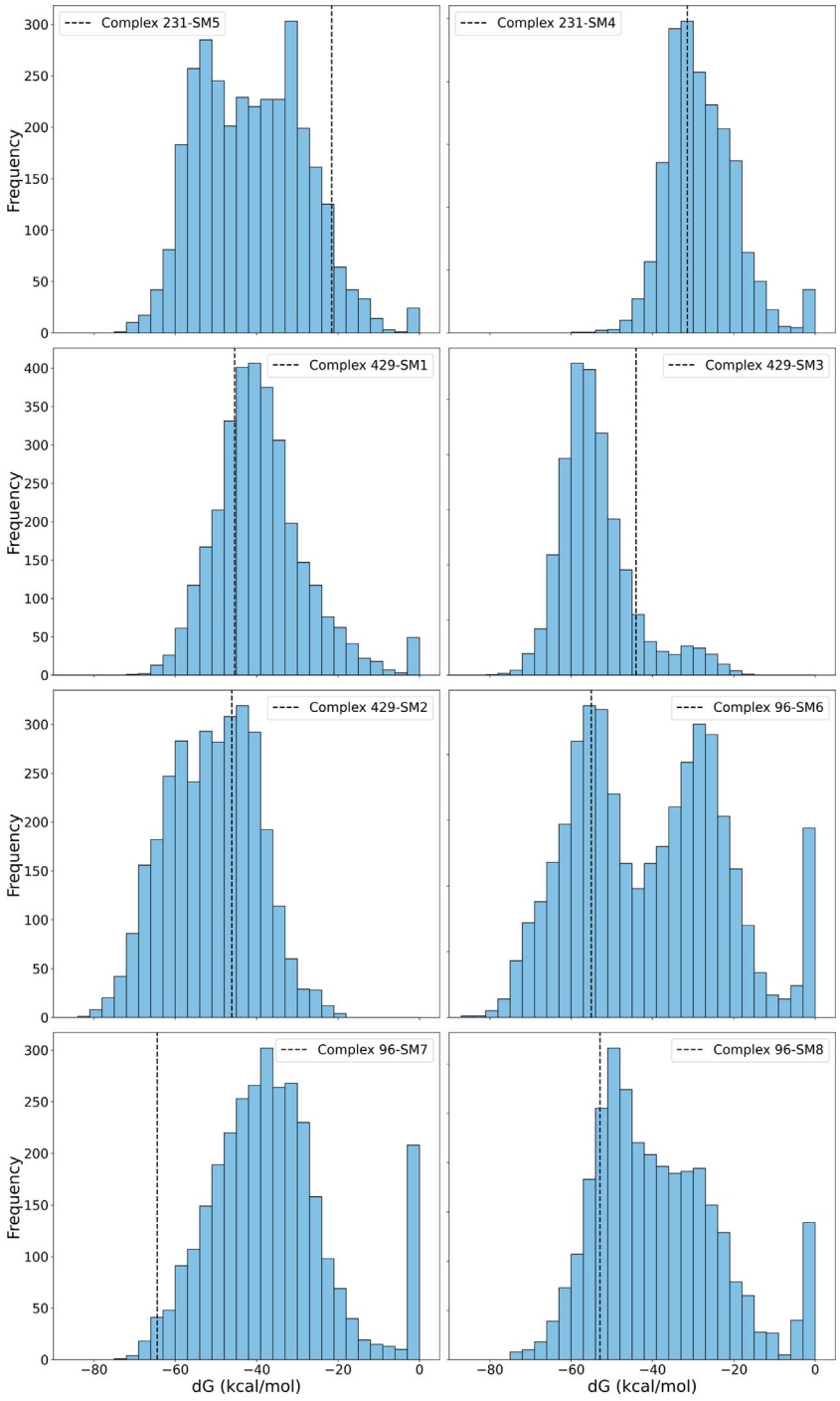

Fig. 7. Distribution of the calculated ΔG values obtained from MM-GBSA calculations. The black dashed line indicates the binding free energy of the initial complex from the MD simulation, corresponding to the docking-derived binding pose.

and conformational heterogeneity require ligands capable of adapting to dynamic binding surfaces. The ability of these compounds to repeatedly form new interactions may represent a key feature in effectively modulating IDP behavior. As the structure of the peptide–ligand complex undergoes conformational changes without aggregating, it may lose contact with the ligand and revert to a non-fibrillar-prone form, while a non-fibrillar-prone conformation could transform into a fibrillar-prone form, subsequently interacting with another inhibitor molecule. This dynamic behavior reflects the intrinsic flexibility of both Aβ and Aβ-ligand complexes, suggesting that these compounds are particularly well-suited to interact with the multiple conformations of fibrillar-prone Aβ. Such adaptability could be crucial for maintaining a long-term inhibitory effect on aggregation.

5. Conclusions

This study highlights the potential of targeting fibrillar-prone forms of Aβ as a therapeutic strategy to mitigate amyloid-related toxicity. By leveraging structural insights and computational approaches, we identified distinct fibrillar-prone conformations and their associated binding sites. Molecular dynamics simulations confirmed the dynamic nature of interactions between Aβ and the selected small molecules. This adaptability underscores the flexibility of these compounds in

engaging with intrinsically disordered targets. Notably, the ability of ligands to maintain binding activity across multiple conformations may represent a critical feature for the successful inhibition of fibrillar-prone aggregation. Compounds such as SM2, SM3, and SM5 have been identified as promising candidates for further studies. These compounds are of particular significance because they not only engage effectively with the target, thereby reducing its propensity to form fibrils, but are also predicted to successfully traverse the BBB, a fundamental characteristic for this category of drugs. As such, they represent a solid foundation for the development of more potent compounds. Additionally, SM6, SM7, and SM1, which possess similar properties, are equally worthy of further investigation.

Future work should focus on experimental validation of these findings through in-vitro assays. Additionally, exploring environmental factors, such as pH and ionic strength, could provide a more comprehensive understanding of ligand performance under varying physiological conditions. In conclusion, this study not only proposes a workflow for targeting highly flexible protein structures but also offers valuable insights into the design of small molecules to inhibit amyloid aggregation and its associated toxic effects.

CRediT authorship contribution statement

Stefano Bosio: Writing – review & editing, Writing – original draft, Validation, Software, Investigation, Formal analysis, Data curation. **Federico Falchi:** Writing – review & editing, Writing – original draft, Supervision, Methodology, Investigation, Formal analysis, Data curation. **Chiara Rauzi:** Investigation, Formal analysis, Data curation. **Luca Bellucci:** Writing – review & editing, Writing – original draft, Supervision, Methodology, Investigation, Data curation, Conceptualization.

Declaration of Generative AI and AI-assisted Technologies in the Writing Process

During the preparation of this work the authors used ChatGPT in order to improve the readability and language of the manuscript. After using this tool, the authors reviewed and edited the content as needed and take full responsibility for the content of the published article.

Fundings

This research did not receive any specific grant from funding agencies in the public, commercial, or not-for-profit sectors.

Declaration of competing interest

The authors declare that they have no known competing financial interests or personal relationships that could have appeared to influence the work reported in this paper.

Appendix A. Supplementary data

Supporting Information includes: MM-GBSA details,3D representation of structure 346, Table of conversions between commercial IDs and custom IDs for the small molecules presented in this study, 2D representations of the selected molecules, Table containing all details related to pocket identification and analysis, Analysis of sites 117 and 78, 3D representation of the HADDOCK output, MM-GBSA timeseries.

Supplementary material related to this article can be found online at https://doi.org/10.1016/j.compbiomed.2025.110545.

References

[1] V.A. Ciurea, R.-A. Covache-Busuioc, A.G. Mohan, H.P. Costin, V. Voicu, Alzheimer's disease: 120 years of research and progress, J. Med. Life 16 (2) (2023) 173.

[2] M. Goedert, M.G. Spillantini, A century of Alzheimer's disease, Sci. 314 (5800) (2006) 777–781, http://dx.doi.org/10.1126/science.1132814.

[3] J. Habchi, P. Tompa, S. Longhi, V.N. Uversky, Introducing protein intrinsic disorder, Chem. Rev. 114 (13) (2014) 6561–6588.

[4] P.H. Nguyen, A. Ramamoorthy, B.R. Sahoo, J. Zheng, P. Faller, J.E. Straub, L. Dominguez, J.-E. Shea, N.V. Dokholyan, A. De Simone, et al., Amyloid oligomers: A joint experimental/computational perspective on Alzheimer's disease, Parkinson's disease, type II diabetes, and amyotrophic lateral sclerosis, Chem. Rev. 121 (4) (2021) 2545–2647.

[5] J. Hardy, D.J. Selkoe, The amyloid hypothesis of Alzheimer's disease: progress and problems on the road to therapeutics, Sci. 297 (5580) (2002) 353–356.

[6] D.J. Selkoe, J. Hardy, The amyloid hypothesis of Alzheimer's disease at 25 years, EMBO Mol. Med. 8 (6) (2016) 595–608.

[7] I.W. Hamley, The amyloid beta peptide: a chemist's perspective. Role in Alzheimer's and fibrillization, Chem. Rev. 112 (10) (2012) 5147–5192.

[8] S.I. Cohen, S. Linse, L.M. Luheshi, E. Hellstrand, D.A. White, L. Rajah, D.E. Otzen, M. Vendruscolo, C.M. Dobson, T.P. Knowles, Proliferation of amyloid-β42 aggregates occurs through a secondary nucleation mechanism, Proc. Natl. Acad. Sci. 110 (24) (2013) 9758–9763.

[9] I. Benilova, E. Karran, B. De Strooper, The toxic Aβ oligomer and Alzheimer's disease: an emperor in need of clothes, Nature Neurosci. 15 (3) (2012) 349–357.

[10] G. Fusco, S.W. Chen, P.T. Williamson, R. Cascella, M. Perni, J.A. Jarvis, C. Cecchi, M. Vendruscolo, F. Chiti, N. Cremades, et al., Structural basis of membrane disruption and cellular toxicity by α-synuclein oligomers, Sci. 358 (6369) (2017) 1440–1443.

[11] C. Mollinari, A. Cardinale, L. Lupacchini, A. Martire, V. Chiodi, A. Martinelli, A.M. Rinaldi, M. Fini, S. Pazzaglia, M.R. Domenici, et al., The DNA repair protein DNA-PKcs modulates synaptic plasticity via PSD-95 phosphorylation and stability, EMBO Rep. 25 (8) (2024) 3707–3737.

[12] G. Brancolini, L. Bellucci, M.C. Maschio, R. Di Felice, S. Corni, The interaction of peptides and proteins with nanostructures surfaces: a challenge for nanoscience, Curr. Opin. Colloid Interface Sci. 41 (2019) 86–94.

[13] L. Bellucci, G. Bussi, R. Di Felice, S. Corni, Fibrillation-prone conformations of the amyloid-β-42 peptide at the gold/water interface, Nanoscale 9 (6) (2017) 2279–2290.

[14] M. Mahmoudi, H.R. Kalhor, S. Laurent, I. Lynch, Protein fibrillation and nanoparticle interactions: opportunities and challenges, Nanoscale 5 (7) (2013) 2570–2588.

[15] S. Laurent, M.R. Ejtehadi, M. Rezaei, P.G. Kehoe, M. Mahmoudi, Interdisciplinary challenges and promising theranostic effects of nanoscience in Alzheimer's disease, RSC Adv. 2 (12) (2012) 5008–5033.

[16] L. Fei, S. Perrett, Effect of nanoparticles on protein folding and fibrillogenesis, Int. J. Mol. Sci. 10 (2) (2009) 646–655.

[17] R. Vacha, S. Linse, M. Lund, Surface effects on aggregation kinetics of amyloidogenic peptides, J. Am. Chem. Soc. 136 (33) (2014) 11776–11782.

[18] H. Lu, L. Bellucci, S. Sun, D. Qi, M. Rosa, R. Berger, S. Corni, M. Bonn, Acidic PH promotes refolding and macroscopic assembly of amyloid β (16–22) peptides at the air–water interface, J. Phys. Chem. Lett. 13 (29) (2022) 6674–6679.

[19] T. John, J. Adler, C. Elsner, J. Petzold, M. Krueger, L.L. Martin, D. Huster, H.J. Risselada, B. Abel, Mechanistic insights into the size-dependent effects of nanoparticles on inhibiting and accelerating amyloid fibril formation, J. Colloid Interface Sci. 622 (2022) 804–818.

[20] H. Okumura, Perspective for molecular dynamics simulation studies of amyloid-β aggregates, J. Phys. Chem. B 127 (51) (2023) 10931–10940.

[21] B. Strodel, Amyloid aggregation simulations: challenges, advances and perspectives, Curr. Opin. Struct. Biol. 67 (2021) 145–152.

[22] Y. Zhang, H. Chen, R. Li, K. Sterling, W. Song, Amyloid β-based therapy for Alzheimer's disease: Challenges, successes and future, Signal Transduct. Target. Ther. 8 (1) (2023) 248.

[23] M.A. Mintun, A.C. Lo, C. Duggan Evans, A.M. Wessels, P.A. Ardayfio, S.W. Andersen, S. Shcherbinin, J. Sparks, J.R. Sims, M. Brys, et al., Donanemab in early Alzheimer's disease, N. Engl. J. Med. 384 (18) (2021) 1691–1704.

[24] J.R. Sims, J.A. Zimmer, C.D. Evans, M. Lu, P. Ardayfio, J. Sparks, A.M. Wessels, S. Shcherbinin, H. Wang, E.S.M. Nery, et al., Donanemab in early symptomatic Alzheimer disease: the trailblazer-ALZ 2 randomized clinical trial, Jama 330 (6) (2023) 512–527.

[25] S. Budd Haeberlein, P. Aisen, F. Barkhof, S. Chalkias, T. Chen, S. Cohen, G. Dent, O. Hansson, K. Harrison, C. Von Hehn, et al., Two randomized phase 3 studies of aducanumab in early Alzheimer's disease, J. Prev. Alzheimer's Dis. 9 (2) (2022) 197–210.

[26] A. Rahman, M.A. Hossen, M.F.I. Chowdhury, S. Bari, N. Tamanna, S.S. Sultana, S.N. Haque, A. Al Masud, K. Saif-Ur-Rahman, Aducanumab for the treatment of Alzheimer's disease: a systematic review, Psychogeriatrics 23 (3) (2023) 512–522.

[27] K.G. Yiannopoulou, S.G. Papageorgiou, Current and future treatments in Alzheimer disease: an update, J. Central Nerv. Syst. Dis. 12 (2020) 1179573520907397.

[28] D. Jeremic, L. Jiménez-Díaz, J.D. Navarro-López, Past, present and future of therapeutic strategies against amyloid-β peptides in Alzheimer's disease: A systematic review, Ageing Res. Rev. 72 (2021) 101496.

[29] A. Battisti, A.P. Piccionello, A. Sgarbossa, S. Vilasi, C. Ricci, F. Ghetti, F. Spinozzi, A.M. Gammazza, V. Giacalone, A. Martorana, et al., Curcumin-like compounds designed to modify amyloid beta peptide aggregation patterns, RSC Adv. 7 (50) (2017) 31714–31724.
[30] G. Toth, S.J. Gardai, W. Zago, C.W. Bertoncini, N. Cremades, S.L. Roy, M.A. Tambe, J.-C. Rochet, C. Galvagnion, G. Skibinski, et al., Targeting the intrinsically disordered structural ensemble of α-synuclein by small molecules as a potential therapeutic strategy for Parkinson's disease, PloS One 9 (2) (2014) e87133.
[31] D.I. Hammoudeh, A.V. Follis, E.V. Prochownik, S.J. Metallo, Multiple independent binding sites for small-molecule inhibitors on the oncoprotein c-Myc, J. Am. Chem. Soc. 131 (21) (2009) 7390–7401.
[32] A.V. Follis, D.I. Hammoudeh, A.T. Daab, S.J. Metallo, Small-molecule perturbation of competing interactions between c-Myc and max, Bioorg. Med. Chem. Lett. 19 (3) (2009) 807–810.
[33] T. Berg, Small-molecule modulators of c-Myc/Max and Max/Max interactions, Small-Mol. Inhib. Protein-Protein Interact. (2010) 139–149.
[34] G.T. Heller, F.A. Aprile, T.C. Michaels, R. Limbocker, M. Perni, F.S. Ruggeri, B. Mannini, T. Löhr, M. Bonomi, C. Camilloni, et al., Small-molecule sequestration of amyloid-β as a drug discovery strategy for Alzheimer's disease, Sci. Adv. 6 (45) (2020) eabb5924.
[35] T. Löhr, K. Kohlhoff, G.T. Heller, C. Camilloni, M. Vendruscolo, A small molecule stabilizes the disordered native state of the Alzheimer's Aβ Peptide, ACS Chem. Neurosci. 13 (12) (2022) 1738.
[36] M. Khaled, I. Rönnbäck, L.L. Ilag, A. Gräslund, B. Strodel, N. Österlund, A hairpin motif in the amyloid-β peptide is important for formation of disease-related oligomers, J. Am. Chem. Soc. 145 (33) (2023) 18340–18354.
[37] D.J. Rosenman, C.R. Connors, W. Chen, C. Wang, A.E. García, Aβ monomers transiently sample oligomer and fibril-like configurations: ensemble characterization using a combined MD/NMR approach, J. Mol. Biol. 425 (18) (2013) 3338–3359.
[38] J. Kutzsche, D. Jürgens, A. Willuweit, K. Adermann, C. Fuchs, S. Simons, M. Windisch, M. Hümpel, W. Rossberg, M. Wolzt, et al., Safety and pharmacokinetics of the orally available antiprionic compound PRI-002: A single and multiple ascending dose phase I study, Alzheimer's Dement.: Transl. Res. Clin. Interv. 6 (1) (2020) e12001.
[39] A. Willuweit, S. Humpert, M. Schöneck, H. Endepols, N. Burda, L. Gremer, I. Gering, J. Kutzsche, N.J. Shah, K.-J. Langen, et al., Evaluation of the 18F-labeled analog of the therapeutic all-D-enantiomeric peptide RD2 for amyloid β imaging, Eur. J. Pharm. Sci. 184 (2023) 106421.
[40] R. Roy, S. Paul, Illustrating the effect of small molecules derived from natural resources on amyloid peptides, J. Phys. Chem. B 127 (3) (2023) 600–615.
[41] J. Bieschke, J. Russ, R.P. Friedrich, D.E. Ehrnhoefer, H. Wobst, K. Neugebauer, E.E. Wanker, EGCG remodels mature α-synuclein and amyloid-β fibrils and reduces cellular toxicity, Proc. Natl. Acad. Sci. 107 (17) (2010) 7710–7715.
[42] C. Wu, J. Scott, J.-E. Shea, Binding of Congo red to amyloid protofibrils of the Alzheimer Aβ9–40 peptide probed by molecular dynamics simulations, Biophys. J. 103 (3) (2012) 550–557.
[43] R. Paul, S. Bera, M. Devi, S. Paul, Inhibition of Aβ16–22 peptide aggregation by small molecules and their permeation through POPC lipid bilayer: Insight from molecular dynamics simulation study, J. Chem. Inf. Model. 62 (21) (2022) 5193–5207.
[44] L.L.N. Ngoc, S.G. Itoh, P. Sompornpisut, H. Okumura, Replica-permutation molecular dynamics simulations of an amyloid-β (16–22) peptide and polyphenols, Chem. Phys. Lett. 758 (2020) 137913.
[45] D. Fukuhara, S.G. Itoh, H. Okumura, Inhibition of amyloid-β (16–22) aggregation by polyphenols using replica permutation with solute tempering molecular dynamics simulation, Biophys. Phys. 20 (4) (2023) e200045.
[46] J.M. Jakubowski, A.A. Orr, D.A. Le, P. Tamamis, Interactions between curcumin derivatives and amyloid-β fibrils: insights from molecular dynamics simulations, J. Chem. Inf. Model. 60 (1) (2019) 289–305.
[47] Y. Sugita, Y. Okamoto, Replica-exchange molecular dynamics method for protein folding, Chem. Phys. Lett. 314 (1) (1999) 141–151.
[48] W.L. Jorgensen, D.S. Maxwell, J. Tirado-Rives, Development and testing of the OPLS all-atom force field on conformational energetics and properties of organic liquids, J. Am. Chem. Soc. 118 (45) (1996) 11225–11236, http://dx.doi.org/10.1021/ja9621760, arXiv:http://pubs.acs.org/doi/pdf/10.1021/ja9621760, URL http://pubs.acs.org/doi/abs/10.1021/ja9621760.
[49] M.J. Robertson, J. Tirado-Rives, W.L. Jorgensen, Improved peptide and protein torsional energetics with the OPLS-AA force field, J. Chem. Theory Comput. 11 (7) (2015) 3499–3509.
[50] O.C. Weber, V.N. Uversky, How accurate are your simulations? Effects of confined aqueous volume and AMBER FF99sB and CHARMM22/CMAP force field parameters on structural ensembles of intrinsically disordered proteins: Amyloid-β42 in water, Intrinsically Disord. Proteins 5 (1) (2017) e1377813.
[51] T.A. Halgren, Identifying and characterizing binding sites and assessing druggability, J. Chem. Inf. Model. 49 (2) (2009) 377–389.
[52] T. Halgren, New method for fast and accurate binding-site identification and analysis, Chem. Biol. Drug Des. 69 (2) (2007) 146–148.
[53] C. Dominguez, R. Boelens, A.M. Bonvin, HADDOCK: a protein- protein docking approach based on biochemical or biophysical information, J. Am. Chem. Soc. 125 (7) (2003) 1731–1737.
[54] R.V. Honorato, M.E. Trellet, B. Jiménez-García, J.J. Schaarschmidt, M. Giulini, V. Reys, P.I. Koukos, J.P. Rodrigues, E. Karaca, G.C. van Zundert, et al., The HADDOCK2.4 web server for integrative modeling of biomolecular complexes, Nat. Protoc. (2024) 1–23.
[55] R.C. Johnston, K. Yao, Z. Kaplan, M. Chelliah, K. Leswing, S. Seekins, S. Watts, D. Calkins, J. Chief Elk, S.V. Jerome, et al., Epik: p K a and protonation state prediction through machine learning, J. Chem. Theory Comput. 19 (8) (2023) 2380–2388.
[56] S. Rupiani, R. Buonfiglio, M. Manerba, L. Di Ianni, M. Vettraino, E. Giacomini, M. Masetti, F. Falchi, G. Di Stefano, M. Roberti, et al., Identification of N-acylhydrazone derivatives as novel lactate dehydrogenase a inhibitors, Eur. J. Med. Chem. 101 (2015) 63–70.
[57] M. Masetti, F. Falchi, D. Gioia, M. Recanatini, S. Ciurli, F. Musiani, Targeting the protein tunnels of the urease accessory complex: a theoretical investigation, Molecules 25 (12) (2020) 2911.
[58] Y. Yang, K. Yao, M.P. Repasky, K. Leswing, R. Abel, B.K. Shoichet, S.V. Jerome, Efficient exploration of chemical space with docking and deep learning, J. Chem. Theory Comput. 17 (11) (2021) 7106–7119.
[59] R.A. Friesner, J.L. Banks, R.B. Murphy, T.A. Halgren, J.J. Klicic, D.T. Mainz, M.P. Repasky, E.H. Knoll, M. Shelley, J.K. Perry, et al., Glide: a new approach for rapid, accurate docking and scoring. 1. Method and assessment of docking accuracy, J. Med. Chem. 47 (7) (2004) 1739–1749.
[60] T.A. Halgren, R.B. Murphy, R.A. Friesner, H.S. Beard, L.L. Frye, W.T. Pollard, J.L. Banks, Glide: a new approach for rapid, accurate docking and scoring. 2. Enrichment factors in database screening, J. Med. Chem. 47 (7) (2004) 1750–1759.
[61] R.A. Friesner, R.B. Murphy, M.P. Repasky, L.L. Frye, J.R. Greenwood, T.A. Halgren, P.C. Sanschagrin, D.T. Mainz, Extra precision glide: Docking and scoring incorporating a model of hydrophobic enclosure for protein- ligand complexes, J. Med. Chem. 49 (21) (2006) 6177–6196.
[62] K.J. Bowers, E. Chow, H. Xu, R.O. Dror, M.P. Eastwood, B.A. Gregersen, J.L. Klepeis, I. Kolossvary, M.A. Moraes, F.D. Sacerdoti, et al., Scalable algorithms for molecular dynamics simulations on commodity clusters, in: Proceedings of the 2006 ACM/IEEE Conference on Supercomputing, 2006, pp. 84–es.
[63] W.L. Jorgensen, J. Chandrasekhar, J.D. Madura, R.W. Impey, M.L. Klein, Comparison of simple potential functions for simulating liquid water, J. Chem. Phys. 79 (1983) 926–935.
[64] M. Tuckerman, B.J. Berne, G.J. Martyna, Reversible multiple time scale molecular dynamics, J. Chem. Phys. 97 (3) (1992) 1990–2001.
[65] G.J. Martyna, M.L. Klein, M. Tuckerman, Nosé–Hoover chains: The canonical ensemble via continuous dynamics, J. Chem. Phys. 97 (4) (1992) 2635–2643.
[66] G.J. Martyna, D.J. Tobias, M.L. Klein, Constant pressure molecular dynamics algorithms, J. Chem. Phys. 101 (5) (1994) 4177–4189.
[67] S. Genheden, U. Ryde, The MM/PBSA and MM/GBSA methods to estimate ligand-binding affinities, Expert. Opin. Drug Discov. 10 (5) (2015) 449–461.
[68] S.G. Itoh, M. Yagi-Utsumi, K. Kato, H. Okumura, Key residue for aggregation of Amyloid-β peptides, ACS Chem. Neurosci. 13 (22) (2022) 3139–3151.
[69] M. Bernetti, R. Aguti, S. Bosio, M. Recanatini, M. Masetti, A. Cavalli, Computational drug discovery under RNA times, QRB Discov. 3 (2022) e22.